Carbamates as synthetic anion transport motifs: protonophoric and mitochondrial uncoupling activity of aryl-carbamate substituted fatty acids.

Hugo MacDermott-Opeskin[1], Callum Clarke[2], Ariane Roseblade[2], Ethan Pacchini [2], Ritik Roy[2], Xin Wu,[3]

Charles Cranfield[4], Philip A. Gale[3,5], Megan L. O'Mara[1], Michael Murray[6] and Tristan Rawling[2†]

[1]Research School of Chemistry, College of Science, The Australian National University, Canberra, ACT, 0200, Australia.

[2]School of Mathematical and Physical Sciences, Faculty of Science, University of Technology Sydney, Sydney, NSW, 2007, Australia.

[3]School of Chemistry, The University of Sydney, NSW, 2006, Australia.

[4]School of Life Sciences, Faculty of Science, University of Technology Sydney, Sydney, NSW, 2007, Australia.

[5]The University of Sydney Nano Institute (SydneyNano), The University of Sydney, NSW, 2006, Australia.

[6]Discipline of Pharmacology, School of Medical Sciences, The University of Sydney, NSW 2006, Australia.

[†]Corresponding author

Abstract

Aryl-urea substituted fatty acids are protonophores and mitochondrial uncouplers that utilise a urea-based synthetic anion transport moiety to carry out the protonophoric cycle. Herein we show that replacement of the urea group with carbamate, a functional group not previously reported to possess anion transport activity, produces analogues that retain the activity to their urea counterparts. Thus, the aryl-carbamate substituted fatty acids uncouple oxidative phosphorylation and inhibit ATP production by collapsing the mitochondrial proton gradient. Proton transport proceeds via self-assembly of the deprotonated aryl-carbamates into membrane permeable dimeric species, formed by intermolecular binding of the carboxylate group to the carbamate moiety. These results highlight the anion transport capacity of the carbamate functional group.

Introduction

Synthetic anion transporters are molecules that facilitate the movement of anions across lipid membranes, a process that is hindered by the lipophilic core of lipid bilayers.[1, 2] Anion transport can occur through membrane channel formation or via a carrier mechanism in which the anion transporter binds an anion to form complexes that are capable of permeating lipid bilayers.[3] Anion binding commonly occurs through non-covalent interactions between the anion and anion binding units in the transporter, which are often hydrogen bond donors.[4] Urea and thiourea functional groups are among the most common functionalities employed in synthetic anion transporters because of their capacity to complex anions with high affinity through parallel hydrogen bonds.[5] Other hydrogen bonding functional groups employed to date in synthetic anion transporters include squaramides,[6] amides[7] and various N-heterocycles.[8-10]

We recently showed that incorporation of a urea-based anion transport moiety into a fatty acid produced a new class of atypical protonophores (termed aryl-ureas, Figure 1) that act as mitochondrial uncouplers and inhibit cellular ATP production.[11] Mitochondria produce ATP through oxidative phosphorylation, a process that couples nutrient oxidation to ATP synthesis through a transmembrane proton gradient. As nutrients are oxidised in the mitochondrial matrix, the energy released is used to pump protons from the mitochondrial matrix into the intermembrane space by a series of proteins embedded in the mitochondrial inner membrane (MIM), thereby establishing a proton gradient across the MIM. This gradient drives the flow of protons through the MIM embedded protein ATP-synthase, which converts ADP to ATP. Mitochondrial uncoupling can occur when protonophores, which are typically lipophilic weak acids, short circuit this mechanism by transporting protons across the MIM and into the matrix through the protonophoric cycle shown in Figure 1a.[12] In this typical protonophoric cycle the protonophore anion (A-, Figure 1a) accepts a proton in the intermembrane space to form a neutral species (A-H) that readily crosses the MIM. Deprotonation of the protonophore in the more alkaline mitochondrial matrix result in the transport of one proton across the MIM and regenerates

the anionic species (A⁻) that must permeate the lipophilic core of the MIM for continued cycling. Thus, the acidic groups in protonophores are most often conjugated to extended π-systems that delocalise charge to promote membrane permeability of the anionic protonophore and further cycling. Aryl-urea substituted fatty acids are of particular interest as they function through an atypical mechanism wherein the acidic group is not directly conjugated with a π-system (Figure 1b). To permeate the MIM after deprotonation of the aryl-urea carboxylic acid group in the matrix, the aryl-ureas self-assemble into membrane permeable dimers, formed by intermolecular interaction of the fatty acid carboxylate group with the urea-based anion transport moiety (Figure 1c).[13, 14] These dimers can return to the intermembrane space, where complex dissociation allows for continued cycling. Thus, the protonophoric and mitochondrial uncoupling activity of the aryl-ureas is directly linked to the carboxylate transport capacity of the synthetic anion transport group.
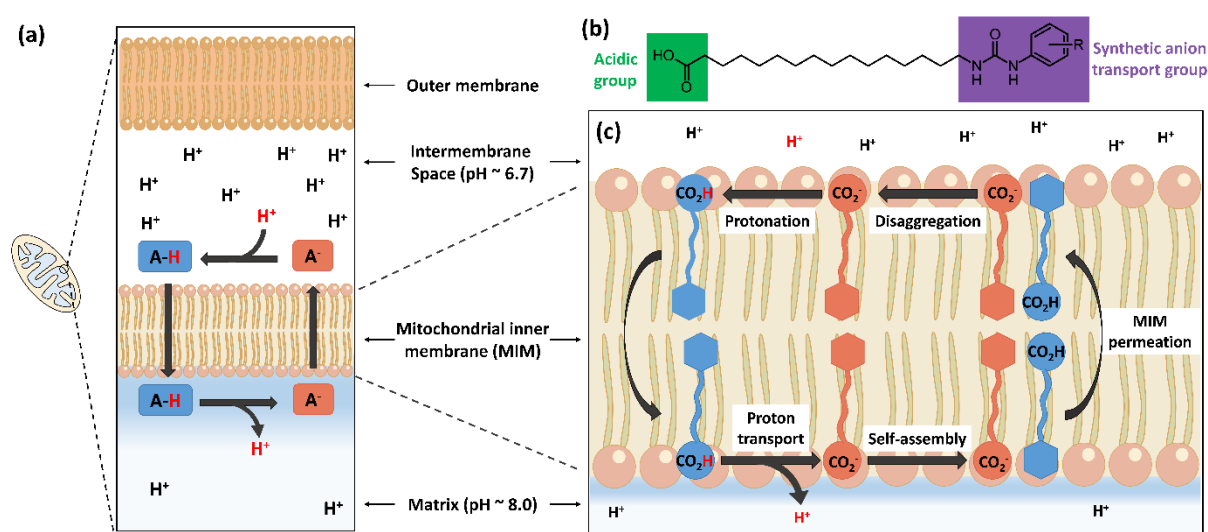

Figure 1. Mitochondrial uncoupling mechanisms of weak acid protonophores and aryl urea substituted fatty acids. Panel (a): Proton transport across the mitochondrial inner membrane (MIM) in the protonophoric cycle. The protonophore (A⁻) is protonated in the intermembrane space, generating a neutral species that freely permeates the MIM. Proton transport occurs when the protonophore is deprotonated in the relatively alkaline matrix. The rate determining step in the cycle

is permeation of the anionic species across the MIM, which allows the cycle to continue; Panel (b): chemical structure of the aryl urea substituted fatty acids; Panel (c): Protonophoric cycle of the aryl urea substituted fatty acids. MIM permeation occurs via self-assembly into membrane permeable dimers formed by carboxylate binding to a urea-based anion transport group.
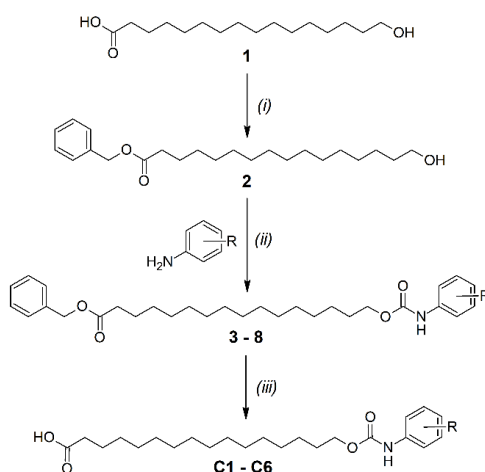
In this paper we replaced the anion transport group in the aryl-urea scaffold with carbamate groups, and studied the anion-binding, protonophoric and mitochondrial uncoupling activities of these compounds using a range of chemical, biological and computational techniques. The carbamate functional group has been used in anion binding studies[15, 16] but has, to the best of our knowledge, not been assessed for anion transport activity. The carbamates were shown to depolarise mitochondria with similar potency to their aryl-urea counterparts. Using experimental and computational approaches we show that the carbamate analogues, like the aryl-ureas, self-associate into anionic dimers that can permeate the MIM. Together these results establish the anion transport capacity of the carbamate functional group for the first time.

Results and discussion:

Compound Design and Synthesis

The protonophoric and mitochondrial uncoupling activity of the aryl-ureas is dependent on the anion transport capacity of the aryl-urea group. Substitution of the aromatic ring with lipophilic electron withdrawing groups was demonstrated to be critical to activity.[11] Electron withdrawing groups increase the acidity and carboxylate affinity of the urea N-H groups to promote dimer formation, and lipophilic substituents increased the membrane permeability of the dimers. Thus, aryl-carbamate substituted fatty acids **C1** - **C6** were substituted with lipophilic electron withdrawing groups.

C1 - **C6** were synthesised in 3 steps as shown in Scheme 1. In the first step the carboxylic acid group in **1** was benzyl-ester protected by reaction with benzyl bromide with caesium carbonate as base. Carbamates **3-8** were prepared from **2** in a two-step, one-pot reaction. Appropriately substituted anilines were first reacted with *N,N*-carbonyldiimidazole to form intermediate *N*-carbamoylimidazoles. These intermediates serve as masked isocyanates,[17] which were then reacted with **2** to form carbamates **3-8**. Removal of the benzyl-protecting groups in **3-8** by palladium-catalysed hydrogenation yielded carbamates **C1**-**C6**.
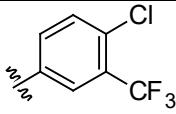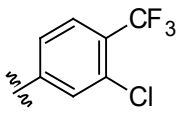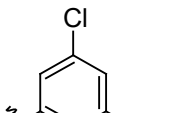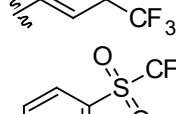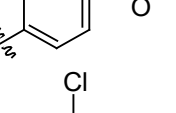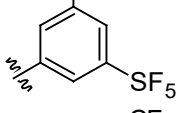

Scheme 1 Synthesis of carbamates **C1**-**C6**. Reagents and conditions: (i) anhydrous DMF, Cs_2CO_3, benzyl bromide, 60 °C, 18 h; (ii) *N,N*-carbonyldiimidazole, anhydrous dichloromethane, rt, 2 h, then rt, 18 h; (iii) anhydrous tetrahydrofuran, H_2, palladium/charcoal, rt, 18 h.

Effects of C1 – C6 on mitochondrial function in MDA-MB-231 cells

Like typical protonophores, the aryl-ureas can uncouple oxidative phosphorylation and inhibit ATP production by collapsing the proton gradient across the MIM. We therefore assessed the protonophoric and mitochondrial uncoupling activity of carbamates **C1** - **C6** in MDA-MB-231 breast cancer cells. Effects on the proton gradient across the MIM were measured using the JC-1 assay. JC-1 is a fluorescent dye that forms aggregates in the matrix of polarised mitochondria that fluoresce red. In response to depolarisation of the MIM JC-1 disaggregates to monomers that diffuse in the cell cytosol and fluoresce green. The JC-1 IC_{50} was defined as the concentration required to shift the red: green fluorescence ratio by 50% of control cells. As shown in Table 1 (see Figure S1 for dose-response plots) carbamates **C1** - **C6** effectively depolarised mitochondria and shifted the JC-1 red: green fluorescence ratio with IC_{50} concentrations between 3-9 µM. The para-substituted analogue **C4** was the least potent in the series (IC_{50} = 8.3 ± 1.1 µM), while the remaining analogues had similar IC_{50} concentrations of ~ 4-5 µM. Interestingly, the JC-1 IC_{50} concentrations observed for the carbamates were very similar to those determined for the corresponding aryl-ureas **U1**-**U6** recorded under identical experimental conditions (see Table 1).[11] For example, the IC_{50} for the 4-Cl, 3-CF$_3$-substituted aryl-urea **U1** was 4.5 ± 1.1 µM[11] while that for its carbamate counterpart **C1** was 4.2 ± 0.1 µM.

Table 1 - Chemical structures and JC-1 IC_{50} concentrations of carbamates **C1-C6** and ureas **U1- U6** measured in MDA-MB-231 cells.

R	Carbamate series		Urea series	
	Compound	JC-1 IC_{50} (µM)	Compound	JC-1 IC_{50} (µM)
	C1	4.2 ± 0.1	U1	4.5 ± 1.1[a]
	C2	4.3 ± 1.7	U2	7.2 ± 1.2[a]
	C3	5.0 ± 1.0	U3	2.9 ± 1.1[a]
	C4	8.3 ± 1.1	U4	6.4 ± 1.2[a]
	C5	3.9 ± 0.4	U5	6.0 ± 1.0[a]
	C6	4.6 ± 0.9	U6	7.6 ± 1.2[a]

[a] IC_{50} concentrations taken from reference [11].

The enzymatic activity of ATP-synthase is dependent upon the proton gradient across the MIM; thus depolarisation of the MIM should inhibit cellular ATP production. We therefore assessed the ability of the **C1** - **C6** to inhibit ATP synthesis in MDA-MB-231 cells. It was anticipated that ATP production would be impaired at concentrations above the JC-1 IC_{50}, where significant proton transport and collapse of the proton gradient across the MIM occurs. As expected, carbamates **C1** - **C6** inhibited ATP production at concentrations above their JC-1 IC_{50} values, (10 and 20 µM, Figure 2a). Consistent with the JC-1 data, **C4** was the least active of the carbamates and decreased ATP formation to 46.7 ± 6.5 % of control values at 20 µM. To confirm that the reductions in intracellular ATP mediated by **C1** - **C6** were not due

to cell death we measured LDH release, which is a cytosolic enzyme that is released by cells during death. **C1-C6** did not significantly increase LDH release relative to control (Figure S2), which suggests that the observed decreases in ATP were due to mitochondrial uncoupling and not cell death.
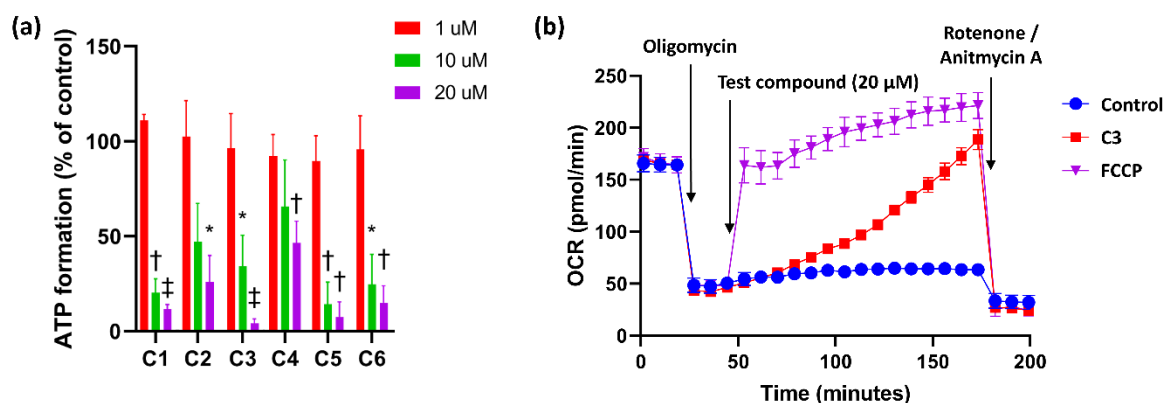

Figure 2 - Effects of carbamates **C1** - **C6** on mitochondrial function in MDA-MB-231 breast cancer cells. (a) ATP formation by MDA-MB-231 cells after 48h treatments with test compounds. Data represents mean ± SEM from three independent experiments. Difference from DMSO treated control: (‡) $P < 0.001$, (†) $P < 0.01$, (*) $P < 0.05$. (b) Oxygen consumption rates (OCR) in MDA-MB-231 cells after sequential addition of the ATP-synthase inhibitor oligomycin (1 µM), protonophore FCCP (1 µM) or test compound (**C3**, 20 µM), and then the ETC complex inhibitors rotenone/antimycin A (1 µM).

The mitochondrial effects observed in JC-1 and ATP assays suggested that carbamates **C1** - **C6** possess uncoupling activity similar to that of the aryl-ureas. To confirm this the uncoupling activity of carbamate **C3** was assessed using the Seahorse Mito Stress test, which directly measures the oxygen consumption rate (OCR) of cells. In the assay MDA-MB-231 cells were treated with the ATP-synthase inhibitor oligomycin, which results in a decrease in OCR. Addition of an uncoupler under these conditions causes an increase in OCR. As shown in Figure 2b, addition of the established protonophore FCCP to oligomycin-treated cells lead to a rapid increase in OCR, consistent with its uncoupling activity. Under the same conditions **C3** also increased OCR, albeit with a slower rate of onset than FCCP. The

differences in kinetics may result from differential subcellular localisation, with the more lipophilic **C3** (cLogP = 7.85, Table S3) initially distributing to the plasma membrane before the mitochondria (FCCP cLogP = 3.71[12]). Regardless, the observed increase in OCR confirms the uncoupling activity of **C3**.

Anion binding and self-association studies

We next undertook mechanistic studies to determine if the carbamates elicited their protonophoric and uncoupling effects by the same mechanism as the aryl-ureas. Analogous aryl-ureas possess uncoupling activity because they self-associate into MIM-permeable dimers following deprotonation in the matrix that enable their return to the intermembrane space and allow for continued protonophoric cycling. Dimerisation is driven by intermolecular interaction of the carboxylate tail with the urea-based anion transport group of an adjacent aryl-urea molecule.

To experimentally assess the carboxylate affinity of the carbamate motif in comparison to the urea motif, we determined acetate (AcO⁻) binding constants of methyl *N*-phenylcarbamate and 1-methyl-3-phenylurea in CDCl$_3$ by integration of ^{1}H NMR signals from the bound AcO⁻ and free AcO⁻ and the host (Figures S3, S4). Methyl *N*-phenylcarbamate bound AcO⁻ with a substantially weaker affinity (320 M^{-1}) than 1-methyl-3-phenylurea (> 2000 M^{-1}), consistent with the lack of a second NH hydrogen bonding site in the carbamate motif.

To assess the capacity of the aryl-carbamates to self-associate, concentration-dependent ^{1}H NMR experiments were performed for deprotonated forms of carbamate **C3** in CDCl$_3$, using 1 equivalent of tetrabutylammonium hydroxide (TBAOH) for deprotonation of the carboxylic acid group. **C3**-TBAOH was found to self-associate in CDCl$_3$ as evident by the pronounced upfield shifts of two aromatic CH peaks from 7.703 and 7.558 ppm to 7.851 and 7.79 ppm, respectively, by increasing the concentration of **C3**-TBAOH from 50 μM to 1.0 mM (Figure S5). The translational diffusion coefficient of **C3**-TBAOH is similar to that of the previously reported urea-TBAOH analogue[11] at 5.0 mM (Table S1) suggesting that dimer was likely the dominant aggregated species.

Dimer formation was also evident in molecular dynamics (MD) simulations of **C3** in a DOPC bilayer (see supporting information for methodology). Both the carboxylic acid (**C3**) and carboxylate (**C3-D**) protomers were examined, as well as systems containing a mix of protomers. All simulated compounds readily embedded themselves in the upper leaflet of the DOPC bilayer. Carboxylic acid **C3** was observed to readily flip between leaflets during the simulation, while carboxylate **C3-D** was confined to the upper leaflet by its anionic tail. Formation of same protomer and cross protomer (Figure 3) dimeric species was readily observed in the DOPC membrane environment, indicating the possible formation of head to tail dimeric species in the MIM. Although these dimeric species were not seen to transit between leaflets on the simulation timescale, it should be noted that in our MD simulations the bilayer lacked the charge gradient that drives anion permeation across the MIM in polarised mitochondria.
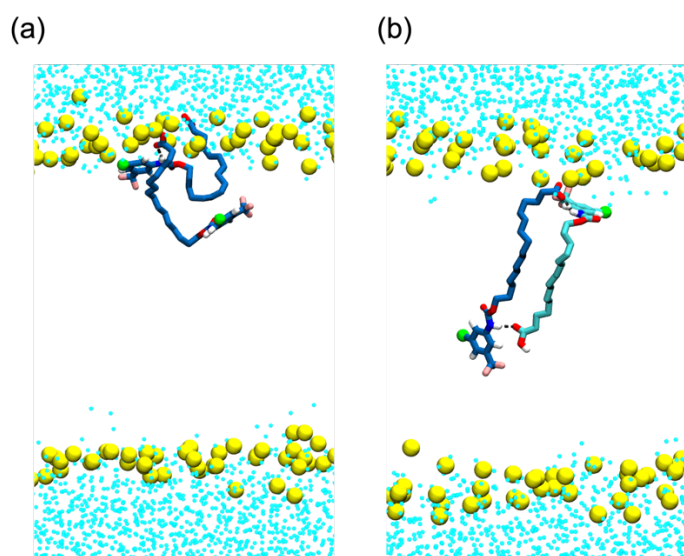

Figure 3. Snapshots from molecular dynamics simulations of **C3**, and the carboxylate equivalent **C3-D** in a DOPC bilayer. Formation of dimeric assemblies is evident in systems containing a) **C3-D**, shown in blue liquorice representation, and b) **C3** and **C3-D**, shown in blue and cyan liquorice representation respectively. Water is shown as blue dots and the lipid headgroup phosphates are shown as yellow spheres.

To further understand the capacity of the carbamates and amides to carry out the carboxylate binding step, double hybrid DFT calculations were employed. Calculations at the DSD-PBEP86/aug-cc-pVTZ//M06-2X-D3(0)/6-311+G(d) level of theory[18, 19] were used to examine the binding energetics of compounds **C1**-**C6** complexed with a model carboxylate (see supporting information for methodology). In addition to **C1**- **C6** the corresponding aryl-urea analogues (**U1**-**U6,** Table 1) were also examined for comparative purposes. Gas phase binding enthalpies revealed that tail-truncated aryl-urea analogues (**U1**-**U6**) bound a model carboxylate (propanoate) with greater affinity (-161.70 kJ/mol average, Table S2) compared to carbamates **C1**-**C6** (107.92 kJ/mol average, Table S2). Trends in gas phase affinities were reflected in implicit solvent with the aryl-urea > aryl-carbamate ordering preserved in both water and a non-polar solvent n-pentadecane (Table S2). Unfavourable binding enthalpies in water (8.79, and 9.97 kJ/mol average for **U** and **C** series respectively) indicate facile dissociation of the carboxylate and anion binding motif in water. Additionally, favourable binding enthalpies in n-pentadecane (-95.74 and -56.70 kJ/mol average for **U** and **C** series, respectively) suggest strong association of the carboxylate and anion binding motif in a low dielectric medium, such as the interior of the MIM. Trends in binding enthalpies can be rationalised through examination of carboxylate coordination geometries across the aryl-urea and aryl-carbamate series exemplified by **C3** and the corresponding aryl-urea (**U3**) in Figure 4. As expected,[5, 20] **U3** donates two parallel N-H hydrogen bonds to the carboxylate moiety resulting in a bidentate coordination mode (Figure 4a). **C3** also donates two hydrogen bonds to the carboxylate moiety, an aryl C-H hydrogen bond and an N-H hydrogen bond from the carbamate moiety (Figure 4b). Aryl C-H hydrogen bonds are generally weaker than N-H hydrogen bonds, accounting for the lower propanoate binding enthalpies of aryl-carbamates compared to aryl-ureas.[21]
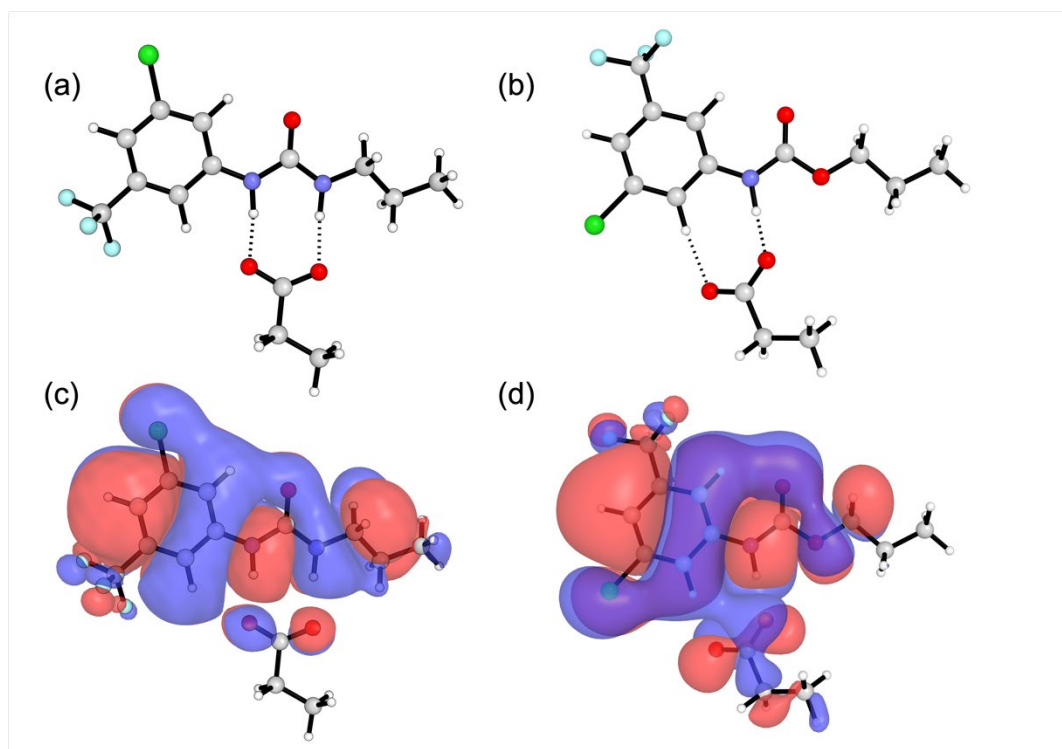
Figure 4. Geometries of 3-chloro, 5-triflouromethyl-substituted urea (**U3**), panel a) and carbamate (**C3**, panel b) analogues complexed to propanoate. The HOMO of the resulting anionic complex is shown in panels c) and d) respectively. Geometries were optimized at the M06-2X-D3(0)/6-311+G(d) level of theory. Molecular orbital plots were constructed from a DSD-PBEP86/aug-cc-pVTZ single-point and contoured at the 0.003 isovalue.

Finally, to confirm that the carbamates in their anionic form permeate bilayers as dimeric species in the protonophoric cycle we measured the concentration dependant effects of **C1** - **C6** on bilayer conductance. A directly proportional relationship between bilayer conductance and protonophore concentration indicates that the membrane permeant species is the monomeric anion, while bilayer conductance increases with the square of the protonophore concentration when an anionic dimer is the permeant species.[22] To perform these studies we utilised tethered bilayer lipid membranes (tBLMs) formed from 1,2-dioleoyl-*sn*-glycero-3-phosphocholine (DOPC), a major lipid component of the MIM[23]. Addition of a protonophore produces an increase in conductance because protons are

transported across the bilayer and are detected by electrical impedance spectroscopy.[11] As shown in Figure S7, carbamates **C1** - **C6** produced an increase in bilayer conductance that was proportional to the square of carbamate concentration, which is consistent dimer formation.

Taken together, these data provide evidence that carbamates **C1** - **C6** uncouple mitochondria and transport protons across lipid bilayers via the dimerisation mechanism first identified for the aryl-ureas. Since mitochondrial uncoupling activity in these scaffolds is directly linked to the carboxylate transport capacity of the synthetic anion transport group, these data show, for the first time that the carbamate functional group can act as synthetic anion transport motif. One surprising observation from the cell data is that carbamates **C1** - **C6** depolarise mitochondria in JC-1 assays with equivalent potencies to their urea counterparts. This result is unexpected because anion affinity has been identified as an important determinant of anion transport capacity,[24] and the experimental and computational data showed that the ureas bind to carboxylate with significant higher affinity. Very high anion affinity can adversely impact anion transport by hindering anion release, therefore it is possible slower anion release by **U1** - **U6** results in equivalent anion transport activity to **C1** - **C6**. This however this is unlikely as hindered anion release has only been observed to affect anion transporters that bind through four or more hydrogen bonds.[25] In addition to anion affinity, lipophilicity[25-28] (expressed as log P) and molecular size also affect anion transporter activity.[25] Molecular size is unlikely to explain the relative activities of the carbamates and ureas as both scaffolds have similar size. Carbamates **C1** - **C6** are more lipophilic than their urea counterparts **U1** - **U6** (see calculated log P values in Table S3 in SI), and although the difference is small (~ 0.7) it may contribute to the surprising activity of **C1** - **C6** relative to **U1** - **U6**.

Another possible explanation for the equal activity of the ureas and carbamates is the capacity of both functional groups to delocalise the charged anion and produce complexes with greater lipophilicity and membrane permeability. Although the effect of charge delocalisation on anion transport has not

been widely studied, molecular orbital analysis did suggest dispersal of the carboxylate charge across the extended π-system of the aryl-ureas promoted uncoupling activity.[11] Examination of the molecular orbitals of carbamate **C3** and urea **U3** complexed to a model carboxylate moiety (propanoate) revealed that **U3**-propanoate and **C3**-propanoate HOMOs show delocalisation of electron density across the aryl π-system (Figure 4c,d). The efficient delocalisation found in **C3**-propanoate is noteworthy given only one traditional hydrogen bond is present. Efficient charge transfer from the carboxylate moiety in the carbamate series is further demonstrated in Natural Population Analysis (NPA)[29] calculations that indicate comparable delocalisation between the carbamate and urea series (Table S4, average difference of 0.012 natural charge units). Thus, it is possible that charge delocalisation contributes to the similar levels of activity for the carbamate and urea series.

Conclusions

In this paper we report on the synthesis and mechanistic evaluation of a series of protonophoric mitochondrial uncouplers consisting of a long chain fatty acid linked with an aryl-carbamate anionophore. Uncoupling activity was established through cell-based assays, and mechanistic studies revealed that like their urea counterparts, the carbamate analogues self-assemble into membrane permeable anionic dimers that allow for protonophoric activity. Despite weaker carboxylate binding enthalpies, carbamates **C1** - **C6** had similar uncoupling activity to their urea counterparts in cell-based assays, which may result from higher carbamate lipophilicity or similar capacity to delocalise charge of its anion guest. This study provides the first experimental evidence to establish the carbamate function group as a synthetic anion transport motif.

Acknowledgements

*Correspondence: Dr Tristan Rawling, School of Mathematical and Physical Sciences, Faculty of Science, University of Technology Sydney, Ultimo, NSW 2007, Australia. Tel: (61-2)-9514-7956, Email: Tristan.Rawling@uts.edu.au

References

1.   A. Ebert, C. Hannesschlaeger, K.-U. Goss and P. Pohl, *Biophys. J.*, 2018, **115**, 1931-1941.

2.   A. P. Davis, D. N. Sheppard and B. D. Smith, *Chem. Soc. Rev.*, 2007, **36**, 348-357.

3.   B. A. McNally, W. M. Leevy and B. D. Smith, *Supramol. Chem.*, 2007, **19**, 29-37.

4.   L. Chen, S. N. Berry, X. Wu, E. N. W. Howe and P. A. Gale, *Chem*, 2020, **6**, 61-141.

5.   V. Blazek Bregovic, N. Basaric and K. Mlinaric-Majerski, *Coord. Chem. Rev.*, 2015, **295**, 80-124.

6.   N. Busschaert, I. L. Kirby, S. Young, S. J. Coles, P. N. Horton, M. E. Light and P. A. Gale, *Angew. Chem. Intl. Ed.*, 2012, **51**, 4426-4430, S4426/4421-S4426/4469.

7.   K. M. Bak, K. Chabuda, H. Montes, R. Quesada and M. J. Chmielewski, *Org. Biomol. Chem.*, 2018, **16**, 5188-5196.

8.   J. Shang, W. Si, W. Zhao, Y. Che, J.-L. Hou and H. Jiang, *Org. Lett.*, 2014, **16**, 4008-4011.

9.   J. T. Davis, P. A. Gale and R. Quesada, *Chem. Soc. Rev.*, 2020, **49**, 6056-6086.

10.   J. T. Davis, O. Okunola and R. Quesada, *Chem. Soc. Rev.*, 2010, **39**, 3843-3862.

11.   T. Rawling, H. MacDermott-Opeskin, A. Roseblade, C. Pazderka, C. Clarke, K. Bourget, X. Wu, W. Lewis, B. Noble, P. A. Gale, M. L. O'Mara, C. Cranfield and M. Murray, *Chem. Sci.*, 2020, **11**, 12677-12685.

12.   E. S. Childress, S. J. Alexopoulos, K. L. Hoehn and W. L. Santos, *J. Med. Chem.*, 2018, **61**, 4641-4655.

13.   X. Wu and P. A. Gale, *J. Am. Chem. Soc.*, 2016, **138**, 16508-16514.

14.   E. N. W. Howe and P. A. Gale, *J. Am. Chem. Soc.*, 2019, **141**, 10654-10660.

15.   Y. Wang, E. Duran, D. Nacionales, A. Valencia, C. Wostenberg and E. R. Marinez, *Tetrahedron Lett.*, 2008, **49**, 6410-6412.

16.   Y. Xia, B. Wu, S. Li, Z. Yang, Y. Liu and X.-J. Yang, *Supramol. Chem.*, 2010, **22**, 318-324.

17. T. Rawling, A. M. McDonagh, B. Tattam and M. Murray, *Tetrahedron*, 2012, **68**, 6065-6070.

18. S. Kozuch and J. M. L. Martin, *Phys. Chem. Chem. Phys.*, 2011, **13**, 20104-20107.

19. Y. Zhao and D. G. Truhlar, *Theor. Chem. Acc.*, 2008, **120**, 215-241.

20. V. Amendola, L. Fabbrizzi and L. Mosca, *Chem. Soc. Rev.*, 2010, **39**, 3889-3915.

21. L. M. Eytel, H. A. Fargher, M. M. Haley and D. W. Johnson, *Chem. Comm.*, 2019, **55**, 5195-5206.

22. S. McLaughlin, *J. Membrane Biol.*, 1972, **9**, 361-372.

23. S. E. Horvath and G. Daum, *Prog. Lipid Res.*, 2013, **52**, 590-614.

24. N. Busschaert, S. J. Bradberry, M. Wenzel, C. J. E. Haynes, J. R. Hiscock, I. L. Kirby, L. E. Karagiannidis, S. J. Moore, N. J. Wells, J. Herniman, G. J. Langley, P. N. Horton, M. E. Light, I. Marques, P. J. Costa, V. Felix, J. G. Frey and P. A. Gale, *Chem. Sci.*, 2013, **4**, 3036-3045.

25. I. Marques, P. M. R. Costa, M. Q. Miranda, N. Busschaert, E. N. W. Howe, H. J. Clarke, C. J. E. Haynes, I. L. Kirby, A. M. Rodilla, R. Perez-Tomas, P. A. Gale and V. Felix, *Phys. Chem. Chem. Phys.*, 2018, **20**, 20796-20811.

26. V. Saggiomo, S. Otto, I. Marques, V. Felix, T. Torroba and R. Quesada, *Chem. Comm.*, 2012, **48**, 5274-5276.

27. M. J. Spooner and P. A. Gale, *Chem. Comm.*, 2015, **51**, 4883-4886.

28. N. J. Knight, E. Hernando, C. J. E. Haynes, N. Busschaert, H. J. Clarke, K. Takimoto, M. Garcia-Valverde, J. G. Frey, R. Quesada and P. A. Gale, *Chem. Sci.*, 2016, **7**, 1600-1608.

29. A. E. Reed, R. B. Weinstock and F. Weinhold, *J. Chem. Phys.*, 1985, **83**, 735-746.